

Observations of 54 Active Galactic Nuclei with the HEGRA System of Cherenkov Telescopes

F. Aharonian¹, A. Akhperjanian⁷, M. Beilicke⁴, K. Bernlöhr¹, H.-G. Börst⁵, H. Bojahr⁶, O. Bolz¹, T. Coarasa², J.L. Contreras³, J. Cortina², S. Denninghoff², V. Fonseca³, M. Girma¹, N. Götting⁴, G. Heinzelmann⁴, G. Hermann¹, A. Heusler¹, W. Hofmann¹, D. Horns¹, I. Jung¹, R. Kankanyan¹, M. Kestel², A. Konopelko¹, H. Kornmeyer², D. Kranich², H. Lampeitl¹, M. Lopez³, E. Lorenz², F. Lucarelli³, O. Mang⁵, D. Mazin^{4,10}, H. Meyer⁶, R. Mirzoyan², A. Moralejo³, E. Ona-Wilhelmi³, M. Panter¹, A. Plyasheshnikov^{1,8}, G. Pühlhofer¹, R. de los Reyes³, W. Rhode⁶, J. Ripken⁴, G. Rowell¹, V. Sahakian⁷, M. Samorski⁵, M. Schilling⁵, M. Siems⁵, D. Sobzynska^{2,9}, W. Stamm⁵, M. Tluczykont⁴, V. Vitale², H.J. Völk¹, C. A. Wiedner¹, and W. Wittek²

¹ Max-Planck-Institut für Kernphysik, Postfach 103980, D-69029 Heidelberg, Germany

² Max-Planck-Institut für Physik, Föhringer Ring 6, D-80805 München, Germany

³ Universidad Complutense, Facultad de Ciencias Físicas, Ciudad Universitaria, E-28040 Madrid, Spain

⁴ Universität Hamburg, Institut für Experimentalphysik, Luruper Chaussee 149, D-22761 Hamburg, Germany

⁵ Universität Kiel, Institut für Experimentelle und Angewandte Physik, Leibnizstraße 15-19, D-24118 Kiel, Germany

⁶ Universität Wuppertal, Fachbereich Physik, Gaußstr.20, D-42097 Wuppertal, Germany

⁷ Yerevan Physics Institute, Alikhanian Br. 2, 375036 Yerevan, Armenia

⁸ On leave from Altai State University, Dimitrov Street 66, 656099 Barnaul, Russia

⁹ Home institute: University Lodz, Poland

¹⁰ Now at (2)

Received ... / Accepted ...

Abstract. A sample of 54 selected Active Galactic Nuclei (AGN) has been observed with the HEGRA stereoscopic system of Cherenkov Telescopes between 1996 and 2002 in the TeV energy regime. The observations were motivated by the positive results obtained for Mkn 421 and Mkn 501. The distances of the selected objects vary over a large range of redshifts between $z = 0.004$ and $z = 0.7$. Among the observed AGN are the meanwhile established TeV-emitting BL Lac type objects H 1426+428 and 1ES 1959+650. Furthermore the BL Lac object 1ES 2344+514 and the radio galaxy M 87 show evidence for a signal on a 4σ level. The observation of 1ES 2344+514 together with the Whipple results firmly establishes this AGN as a TeV source. Several objects (PKS 2155-304, BL Lacertae, 3C 066A) that have been claimed as TeV γ -ray emitters by other groups are included in this data sample but could not be confirmed using data analysed here. The upper limits of several AGN included in this analysis are compared with predictions in the frame-work of SSC models.

Key words. Gamma rays: observations – Galaxies: active – BL Lacertae objects: individual: 1ES 2344+514 – BL Lacertae objects: individual: 1ES 1959+650 – BL Lacertae objects: individual: H 1426+428 – radio galaxies: individual: M 87

1. Introduction

In the commonly adopted view the ‘central engine’ of Active Galactic Nuclei (AGN) consists of a super massive black hole with up to $10^9 M_{\odot}$ surrounded by an accretion disk. Two relativistic plasma outflows (jets) perpendicular to the accretion disk can be observed in some AGN (Rees 1984; Urry & Padovani 1995). So far, γ -rays in the TeV energy regime from AGN have essentially been detected from objects of the BL Lac type, i.e. AGN having their jet pointing close to the observer’s line of sight. Furthermore, all known TeV blazars are X-ray selected BL Lac objects. Recently, the first

detection of TeV γ -rays from the radio galaxy M 87 with the HEGRA Cherenkov telescopes was reported (Aharonian et al. 2003b).

Different models for the production of TeV γ -rays from BL Lac objects have been proposed. In leptonic models the IC mechanism is assumed to produce the TeV emission (e.g. Sikora (2001)), whereas in hadronic models the γ -rays are produced via the interactions of relativistic protons with matter (e.g. Pohl & Schlickeiser (2000)), ambient photons (Mannheim 1993) or magnetic field (Aharonian 2000), or both (Mücke & Protheroe 2001).

The observed TeV emission shows high flux variability on timescales stretching from months to less than an hour. Detailed studies of variability of BL Lac type objects can

Send offprint requests to: M. Tluczykont, e-mail: Martin.Tluczykont@desy.de

contribute to the understanding of their intrinsic acceleration mechanisms (Krawczynski et al. 2001; Aharonian et al. 2002a). The positive results obtained from the observations of the prominent extragalactic sources of TeV γ -rays Mkn 421 (Punch et al. 1992; Petry et al. 1996; Piron et al. 2001) and Mkn 501 (Quinn et al. 1996; Bradbury et al. 1997; Djannati-Ataï et al. 1999) as well as their relevance for the question of the extragalactic background photon field (Aharonian 2001), have motivated further observations of Active Galactic Nuclei with the HEGRA Cherenkov telescopes. In this paper we present the results of dedicated observations of 54 AGN in the years 1996 to 2002 with the stereoscopic system of Cherenkov telescopes. After a brief introduction to the HEGRA Cherenkov telescopes the analyzed data set will be presented followed by a description of the analysis used in this paper and a presentation of the results. The paper closes with a discussion and a summary.

2. The HEGRA Cherenkov telescope system

The HEGRA stereoscopic Cherenkov telescope system (1996-2002) consisted of 5 imaging air Cherenkov telescopes (IACTs) (Daum et al. 1997) used in the stereoscopic observation mode on the Canary island of La Palma (28.75° N, 17.90° W) at an altitude of 2 200 m a.s.l. Additionally, one telescope (not used for the present analysis) was operated in stand-alone mode (Mirzoyan et al. 1994). Each system telescope was equipped with an 8.5 m² tessellated mirror dish of 30 single mirrors with a diameter of 60 cm each, and a camera consisting of 271 photomultiplier tubes (pixels). The HEGRA IACT system was operating at an energy threshold of 0.5 TeV for photons of vertical incidence, with energy and angular resolution of $\Delta E/E = 10 - 20\%$ and 0.1° respectively on an event-by-event basis. The field of view of each system telescope had a diameter of 4.3° . The introduction of the stereoscopic observation technique results in an improvement of the sensitivity of Cherenkov telescopes and especially allows for an effective γ -hadron separation (see below). The performance of the HEGRA system of Cherenkov telescopes can be found in Pühlhofer et al. (2003).

3. Data Set

Observations of 54 objects of the AGN class were carried out from 1996 to 2002, resulting in a total pre-selection exposure time of approx. 1150 hours (not including Mkn 421 and Mkn 501) corresponding to more than one year of continuous observations in moonless nights with the HEGRA IACT system. The total observation time accumulated for Mkn 421 and Mkn 501 amounts to more than 1500 hours. The results of the HEGRA observations from these two objects were presented in different publications (Bradbury et al. 1997; Aharonian et al. 1999a,b,c; Sambruna et al. 2000; Aharonian et al. 2001a,b, 2002a) and are not included in the present work.

Mkn 421 and Mkn 501 excluded, the data set contains 37 objects identified and confirmed as BL Lac type objects, 10 radio galaxies, 4 Seyfert galaxies, 1 quasar and 2 galaxies following the catalogues of Stickel et al. (1994); Padovani & Giommi (1995); Véron-Cetty & Véron (2001).

The object 1ES 0806+524 is one of the BL Lac objects which was proposed by Tinyakov & Tkachev (2001) to coincide with an AGASA UHECR triplet, thus being a candidate for the acceleration of ultra high energy cosmic rays. The distances of the objects vary over a large range of redshifts between $z \approx 0.004$ (M 87) and $z \approx 0.7$ (PKS 0219-164). However, the expected absorption due to pair production of TeV γ -rays with the extragalactic background light (EBL) (Nikishov 1962) ($\gamma_{\text{TeV}} \gamma_{\text{EBL}} \rightarrow e^+e^-$) increases for larger redshifts, thus decreasing the detectability of objects located at large redshifts. Therefore, most of the observed objects were chosen with regard to their low redshift (i.e. $z < 0.2$).

All observations were carried out in the so called ‘wobble’ mode (Aharonian et al. 1997), tracking the telescopes with an offset of 0.5° in declination with respect to the object position, allowing for simultaneous on- and off-source (background) observations. For consecutive runs with a duration of 20 min, the offset sign is reversed in order to avoid systematic effects due to acceptance inhomogeneities in the field of view. The background is estimated (similar to the method used in Aharonian et al. (2003b)) using a ring segment concentric to the camera center at the same radial distance to the camera center as the on-source region (i.e. 0.5°). A segment with opening angle $\eta = 70^\circ$ is excluded from the background region in order to avoid possible contamination from the on-source region. This method makes sure that on- and off-source measurements are both taken with identical radial camera acceptances and allows at the same time large background statistics.

Two a priori cuts on the system trigger rate are applied to each run in order to exclude runs taken under bad weather conditions and to reduce systematic effects in the determination of the excess rate. In a first step a minimum trigger rate of 7 Hz is required. This cut excludes data taken under the worst weather conditions. In a second step, an expected rate, depending on the hardware settings and the zenith angle of the observations is calculated from the parameters of a fit to all data of one period with constant hardware settings (all runs with trigger rate lower than 7 Hz are excluded from this fit). Runs with rates below 80 % of the expected rate are rejected. Additionally, runs with technical problems are excluded. After the application of the above run-selection criteria the total clean data set amounts to an observation time of 1017 hours. In Table 7 all observed objects are listed with J2000 coordinates, redshift and object type ordered by ascending redshift. Additionally the observation time spent on each object as well as the results of the analysis described below are listed.

4. Data Analysis

The Cherenkov light generated by an air shower initiated by a primary γ -ray or hadronic particle is seen as an elliptical image in each triggered camera. Since each telescope has a different viewing angle relative to the shower axis a complete geometrical reconstruction of the air shower is possible with an image analysis of at least two telescopes.

Before the reconstruction of direction and shower core position the following cuts are applied. Reconstructed images with more than 15 defective camera pixels are rejected. A min-

imum amount of light (*size*) of 40 photo-electrons (ph.e.) is required in an image. Images with a distance of the center of gravity to the camera center of more than 78 % of the camera radius are rejected in order to avoid truncation by the camera border.

After application of the above image selection criteria at least three remaining images are required in this analysis for the reconstruction of the direction and the core impact position of an event. This improves the quality of the reconstruction, the angular resolution and the separation between γ -ray and cosmic ray (hadronic background) induced air showers. The stereoscopic technique allows for an event-by-event reconstruction of the direction of the primary particle. Since the shape of the elliptical images also depends on the shower core position, the reconstruction of the shower impact parameter for each telescope provides a means of scaling the individual widths of the elliptical shower images of each telescope with expected widths for γ -ray induced shower images from Monte-Carlo simulations. The mean of the scaled widths is called mscw-parameter and provides a very good γ -hadron separation. This is described in detail in Konopelko et al. (1999a). The optimum cut value for a γ -ray signal search is found to be mscw = 1.1.

For the reconstruction of the direction of the primary particle, algorithm # 3 from Hofmann et al. (1999) is used. The angle $\Delta\Theta = |\Theta_0 - \Theta_r|$ between the object direction Θ_0 and the reconstructed shower axis Θ_r is called the angular distance. In case of a signal from a source with point-like emission, the distribution of the squared angular distance $\Delta\Theta^2$ is expected to accumulate entries at small values starting from 0, i.e. the signal region. The extension and shape of the signal accumulation reflects the angular resolution of the system and depends on the telescope multiplicity, the zenith angle and the hardware setup of the telescope system. Therefore, the cut on the angular distance also depends on the parameters mentioned above. Using data of the well known Crab Nebula, the cut on $\Delta\Theta^2$ is thus optimized individually for different hardware setups, multiplicities and zenith angle intervals. This method takes the dependencies of the angular resolution described above into account and leads to results consistent with earlier analyses. Typical values of the $\Delta\Theta^2$ -cut are 0.008 deg² for events reconstructed with five triggered telescopes (having the best angular resolution) to 0.015 deg² for 3-telescope events. Similarly, the cut on the core impact position slightly depends on the zenith angle (ZA) of the observation. The optimum values found for this cut are 200 m (low ZA), 400 m (medium ZA) and 600 m (high ZA). In Table 1 all selection criteria and cuts are summarized.

Different cuts on $\Delta\Theta^2$ imply different solid angle ratios of on- and off-source region $\alpha = \Omega_{\text{on}}/\Omega_{\text{off}}$ (α -factor) for each subset. Therefore the significance of an excess is calculated using a formula based upon the likelihood Eq. 17 of Li & Ma (1983)

run selection	rate	> 7Hz
	rate deviation	< 20%
	technical problems	–
image selection	# of defective pixels	< 15
	image size	> 40 ph.e.
	distance	< 0.78
event selection	telescope multiplicity	≥ 3
	core distance	< f(subset)
	mscw	< 1.1
	$\Delta\Theta^2$	< f(subset)

Table 1. Selection criteria of the analysis chain. The cuts were optimized individually for all data subsets using data of the well known Crab Nebula (see text). The distance is measured from the center of gravity of the image to the camera center. The entry ‘f(subset)’ indicates that the cut depends on the data subset.

but generalized for data subsets with different α -factors¹:

$$S = \sqrt{2} \times \left[\sum_i N_{\text{on}}^{(i)} \ln \left(\frac{\sum_i N_{\text{on}}^{(i)}}{\sum_i \frac{\alpha_i}{1+\alpha_i} (N_{\text{on}}^{(i)} + N_{\text{off}}^{(i)})} \right) + \sum_i N_{\text{off}}^{(i)} \ln \left(\frac{\sum_i N_{\text{off}}^{(i)}}{\sum_i \frac{1}{1+\alpha_i} (N_{\text{on}}^{(i)} + N_{\text{off}}^{(i)})} \right) \right]^{1/2}$$

The variability of each object is investigated using the Kolmogorov and the Prah test (Kolmogorov 1933; Prah 1999). Both tests result in a significance for burst-like behaviour, given a time sequence of events. The Prah test is especially sensitive to burst-like behaviour with a small duty cycle.

For each object a Crab Nebula γ -rate as expected for identical observational conditions (zenith angle, hardware setup) is calculated from data. These expected rates are used to compute flux values and upper limits on the integral flux following Helene (1983).

5. Results

A distribution of the significances for steady state emission (DC) of all analyzed objects is shown in Figure 1. The distribution follows a Gaussian distribution of mean zero and standard deviation one, as expected in case of a pure background sample, with exceptions from 1ES 1959+650, H 1426+428, 1ES 2344+514 and M 87. In Table 7 a list of all objects analyzed in this work ordered by ascending redshift is shown along with their observation time and upper limits on the integral flux respectively flux values for the most significant objects. The values of the calculated upper limits are found to lie between 2 % and 60 % of the Crab Nebula flux. Comparable upper limits for BL Lac objects were found with observations of the Whipple telescope, ranging from 6 % to 100 % of the Crab Nebula flux (Horan et al. 2003; de la Calle Perez et al. 2003).

¹ In Li & Ma (1983) the significance is derived from the ratio of the conditional probabilities for ‘background assumption’ and ‘signal assumption’. Substituting both assumptions with a sum over data subsets with different α -factors and a straight forward calculation leads to the above generalized formula.

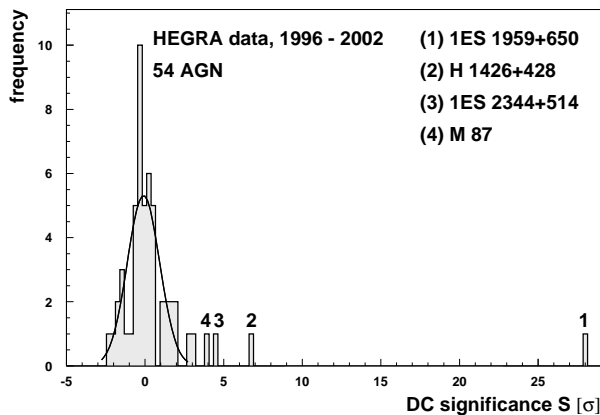


Fig. 1. Distribution of significances for all 54 objects analyzed in this work. A Gaussian fit between -2.5 and $+2.5$ σ matches the core distribution very well. The objects IES 1959+650 and H 1426+428 show a clear deviation from the background expectation. Further two objects, IES 2344+514 and M 87 also show a deviation from the background expectation on the 4σ level and thus evidence for the emission of TeV γ -radiation.

The statistical tests on burst like variability of all objects yield no positive results except for IES 1959+650 where a high statistical significance ($> 16\sigma$) for burst-like behaviour reflects the strong obvious flaring activity in May and July 2002.

The X-ray selected BL Lac object IES 1959+650 (Elvis et al. 1992; Schachter et al. 1993) was first reported as a TeV γ -ray emitter by the Seven Telescope Array group in 1999 with a DC significance of 3.9σ (Nishiyama et al. 1999). HEGRA IACT system observations were carried out from July to September 2000, May to October 2001 and May to September 2002. The HEGRA results on IES 1959+650 were published in detail elsewhere (Aharonian et al. 2003c), the results presented in this analysis show a level of activity ranging from 0.06 to 2.9 Crab units and are consistent with the earlier analysis.

H 1426+428 was reported to have a synchrotron peak lying near or above 100 keV (Costamante et al. 2001) thus qualifying the object as an extreme synchrotron blazar. Detections in the TeV energy regime from this object have been reported by the Whipple collaboration (Horan et al. 2002) the HEGRA collaboration (Aharonian et al. 2002b) and the CAT collaboration (Djannati-Ataï et al. 2002). The observations of H 1426+428 in the years 1999, 2000 and 2002 resulted in an excess on the 7.5σ level (Aharonian et al. 2003a), consistent with the analysis presented here (6.6σ).

IES 2344+514 was one of the first BL Lac type objects to be reported as an extreme synchrotron blazar with synchrotron peak energy reaching up to 100 keV (Giommi et al. 2000). The first TeV detection of this object was reported by the Whipple group in 1998 (Catanese et al. 1998). With an average flux of 11 % of the Crab Nebula flux in 1998 and a higher flux level of 63 % of the Crab flux in one night of observations (6σ), the object has shown clear evidence for a variable flux in the Whipple data. The results of the HEGRA obser-

Table 2. Number of on- and off-source events and significance S for the data sets from the years 1997 (P1), 1998 (P2) and 2002 (P3) on IES 2344+514. Note that the major part of the excess is accumulated in 1998.

observation periods	time [h]	N_{on} #	αN_{off} #	S [σ]
P1 Oct – Dec 1997	15.0	54	52	0.3
P2 Aug – Nov 1998	41.8	128	84	4.3
P3 Sep 2002	15.7	53	35	2.6
Σ	72.5	235	171	4.4

vations on IES 2344+514 of the year 1997 and 1998 were first reported by Konopelko et al. (1999b) with a DC significance of 3.3σ . Further observations have been carried out since the above publication. The analysis presented here includes the complete dataset and results in an excess of 64 ± 15 photons ($N_{\text{on}} = 235$, $\langle N_{\text{off}} \rangle = 171$) with a significance of 4.4σ . The data set of IES 2344+514 can be split into three independent observation periods. The first period P1 ranges from October to December 1997, the second period P2 from August to November 1998. P1 and P2 are separated by a period of non observability of the object from the HEGRA site. Additional observations have been carried out in September 2002 (P3). The data subset P1 shows no evidence for a TeV γ -ray signal, with a DC significance of 0.3σ whereas the second observation period P2 yields a significance of 4.3σ . In the last observation period P3 an excess on the 2.6σ level is found. Tests for burst-like behaviour do not yield statistically significant results. In Table 2 the number of on- and off-source events as well as the corresponding significances are listed for the different data subsamples. In Figure 2 the distributions of the reconstructed directions for the complete data set (P1+P2+P3) and the data set with the highest significance (P2) of IES 2344+514 are shown. The observed excess results in a flux of $\Phi(E>0.97 \text{ TeV}) = (0.60 \pm 0.19) \cdot 10^{-12} \text{ photons cm}^{-2} \text{ s}^{-1}$, corresponding to $(3.3 \pm 1.0)\%$ of the Crab Nebula flux. The errors on the flux level are dominated by the statistics of the measurements.

In contrast to the abovementioned 4 objects the jet of the giant radio galaxy M87 is not aligned to our line of sight which makes it the only non BL Lac type object among the 4 most significant objects of this data sample. The observed excess from the radio galaxy M87 results in a significance of 3.9σ in the present analysis and is consistent to the results of a detailed analysis of the M87 data, which yield 4.1σ and were presented in a dedicated paper (Aharonian et al. 2003b). After further improvements this analysis now yields 4.7σ (Götting et al. 2003).

Several objects that were reported to be sources of TeV γ -rays by other groups are included in this data set. Among these, the objects 3C 066A (Neshpor et al. 1998) and PKS 2155-304 (Chadwick et al. 1999; Djannati-Ataï et al. 2003) were only observed for a very short time. No excess was found in the HEGRA data of these two objects. A weak excess on the 3σ level is found in BL-Lacertae which was observed for 29 hours, resulting in a 99 % C.L. upper limit of the order of 28% of the Crab Nebula flux (see Table 7). This object was reported to be a

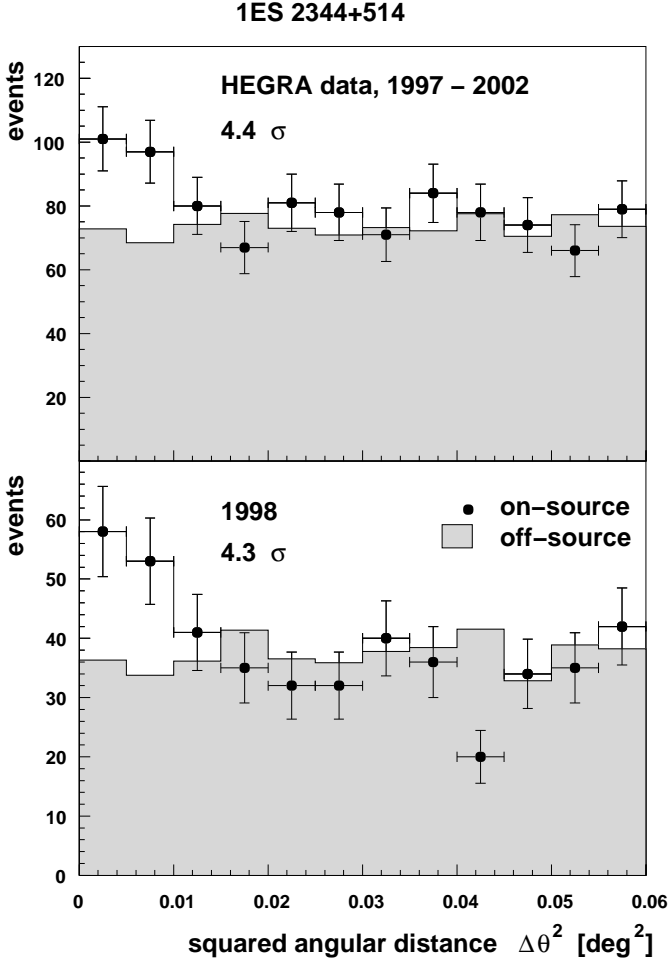


Fig. 2. Distributions of reconstructed squared angular distances to the object direction (see text) of the 1ES 2344+514 data. The distribution of the on-source events is represented by the data points. The scaled background (off) is shown as a shaded histogram. The upper figure represents the total data set taken between 1997 and 2002 whereas the lower figure shows the 1998 data alone. As can be seen from this figure the excess accumulates essentially in the year 1998.

TeV γ -ray emitter by the Crimean Observatory (Neshpor et al. 2001).

6. Discussion

Predictions for γ -ray fluxes in the GeV/TeV energy regime have been made for several AGN by Stecker et al. (1996) and Costamante & Ghisellini (2002).

In Table 3 the observed integral fluxes and flux upper limits of several objects of the present data sample are compared to predictions made by Stecker et al. (1996), based upon simple scaling arguments, taking into account the Einstein Slew survey sample of BL Lacs. The authors argue that only high frequency peaked BL Lac objects are potential sources of extragalactic TeV γ -radiation. For all objects listed in Table 3 the derived HEGRA upper limits on the integral flux were calculated for an energy threshold of 1 TeV and for different spectral indices, assuming a power law energy spectrum. The observed fluxes of

Table 3. Comparison of upper limits and fluxes (Φ) derived in this work with predictions (Φ_{model}) made by Stecker et al. (1996). All fluxes are given in units of 10^{-12} photons $\text{cm}^{-2}\text{s}^{-1}$. The 99% C.L. upper limits were extrapolated to a fixed energy threshold of 1 TeV assuming a power law energy spectrum for 3 differential spectral indices $\alpha = 2.0, 2.5, 3.0$.

object	z	$\Phi_{\text{model}}/10^{-12}$ $\gamma \text{ cm}^{-2} \text{ s}^{-1}$	$\Phi/10^{-12}$ $\gamma \text{ cm}^{-2} \text{ s}^{-1}$		
			spectral index α		
			2.0	2.5	3.0
1Zw 187	0.055	0.59	<1.56	<1.51	<1.47
1ES 2321+419	0.059	0.14	<0.60	<0.56	<0.53
1ES 1741+196	0.083	0.35	<1.33	<1.29	<1.25
PKS 2155-304	0.116	0.88	<1.60	<3.83	<9.16
1ES 1118+424	0.124	0.18	<4.18	<4.12	<4.06
1ES 0145+138	0.125	0.26	<1.19	<1.11	<1.04
1ES 1212+078	0.130	0.03	<2.98	<2.86	<2.74
1ES 0229+200	0.139	0.11	<2.99	<2.87	<2.75
1ES 1255+244	0.140	0.34	<2.03	<1.97	<1.91
1ES 0323+022	0.147	0.15	<0.71	<0.71	<0.71
1ES 1440+122	0.162	0.03	<1.37	<1.31	<1.26
1ES 0347-121	0.185	0.08	<7.50	<9.07	<10.96
1ES 0927+500	0.186	0.02	<1.02	<0.98	<0.95
1ES 2344+514	0.044	0.80	0.58	0.57	0.56
1ES 1959+650	0.047	2.30	1.0 - 51.9		

1ES 1959+650 in its low state and 1ES 2344+514 are close to the predicted values. The calculated HEGRA upper limits for all other objects in this list exceed the predictions. For some objects (e.g. 1ES 0927+500, 1ES 1440+122) the predicted flux levels are a factor of 50 to 100 lower than the upper limits from HEGRA. The level of sensitivity necessary to detect such low fluxes within a reasonable time is beyond the capabilities of the HEGRA Cherenkov telescopes. Such low fluxes could only be detected by the experiments of the next generation which have a higher sensitivity and a lower energy threshold.

In Table 4 the HEGRA integral flux upper limits derived in this work are compared to predictions made by Costamante & Ghisellini (2002). Two different model predictions are given. The first number is taken from a parametrization of the spectral energy distribution (SED) originally introduced by Fossati et al. (1998) and modified by Donato et al. (2001) and Costamante & Ghisellini (2002) (hereafter FDC). The second number is calculated using an SSC model from Costamante & Ghisellini (2002) (hereafter CG). Compared to the earlier work of Stecker et al. (1996), CG introduce the new requirement of strong radio emission for a TeV candidate source (arguing that a strong radio emission is a good indicator for non-thermal low energy emission producing seed photons). Furthermore, several other BL Lac samples in addition to the Einstein Slew survey sample were taken into account. The FDC parametrization is rather suitable for predictions of high state TeV fluxes while the SSC model predictions, designed to fit the known synchrotron part of the SED, are more appropriate for a quiescent state of the TeV source candidate. Additionally, one has to note that along with other uncertainties the absorption of TeV photons by the extragalactic background radiation

Table 4. Comparison of flux predictions by Costamante & Ghisellini (2002) (Φ_{model}) with the results derived in this work. All fluxes are given in units of 10^{-12} photons $\text{cm}^{-2} \text{s}^{-1}$. For the extrapolation of the upper limits given in Table 7 a power law for 3 differential spectral indices ($\alpha = 2.0, 2.5, 3.0$) were assumed and the energy threshold was fixed at $E_{\text{thr}} = 1$ TeV. For 1ES 0647+250 a redshift of 0.200 was assumed. Two numbers for predictions above 1 TeV are given by Costamante & Ghisellini (2002): the first number is obtained from a parametrization of the SED adapted from Fossati et al. (1998) and modified by Donato et al. (2001) and Costamante et al. (2001) (FDC). The second number results from a homogeneous one-zone SSC model described in Costamante & Ghisellini (2002) (CG).

object	z	$\Phi_{\text{model}}/10^{-12}$		$\Phi/10^{-12}$		
		$\gamma \text{ cm}^{-2} \text{ s}^{-1}$		spectral index α		
		FDC	CG	2.0	2.5	3.0
H 1722+119	0.018	35.2	0.01	<3.84	<3.62	< 3.41
1ES 1741+196	0.083	8.4	0.1	<1.33	<1.29	< 1.25
1ES 0806+524	0.138	2.7	–	<4.63	<4.84	< 5.05
1ES 0229+200	0.139	2.1	0.04	<2.99	<2.87	< 2.75
RBS 0958	0.139	2.8	–	<5.30	<4.88	< 4.50
1ES 0323+022	0.147	1.8	–	<0.71	<0.71	< 0.71
1ES 1440+122	0.162	2.0	0.1	<1.37	<1.31	< 1.26
PG 1218+304	0.182	1.5	–	<2.24	<2.06	< 1.88
1ES 0647+250	0.200	1.2	–	<2.61	<2.31	< 2.04
1ES 1011+496	0.200	0.2	–	<1.84	<1.85	< 1.87
1ES 0120+340	0.272	0.6	–	<0.72	<0.66	< 0.60
1ES 1959+650	0.047	17.4	–	1.0 – 51.9		

field was not accounted for in these models (CG). In addition to the flux predictions given in CG, we have used the FDC parametrization to calculate flux predictions for several objects not included in the list of CG. We have additionally included the effect of the absorption of TeV photons by pair production with the extragalactic background light (EBL). For this purpose we have used a model parametrization of the spectral energy distribution of the EBL (also used in Aharonian et al. (2002b), model 1) adopted from Primack (2001) and designed to be consistent with our observations of known TeV Blazars. The luminosity distance was calculated following Ue-Li Pen (1996). These predictions are compared to upper limits calculated in this work in Table 5. In the case of the FDC parametrization, the predicted flux levels exceed the derived upper limits for those objects printed in boldface in Table 4 and Table 5. Assuming these predictions to hold true for a high state of activity, it can be concluded that these objects were not in a flaring state during the HEGRA observations. However, if we take into account the absorption by the EBL (column 4, Table 5) this only remains valid for four objects.

For 1ES 1959+650 the observed flux level during the highest state of emission in the HEGRA data is found to exceed the predicted value by a factor of 3 (only FDC) to 12 (FDC+EBL). Given the high variability of the object at this time, prediction and observation can easily be accommodated. The observed flux from H 1426+428 is roughly a factor of 3

Table 5. Comparison of integral flux predictions above 1 TeV using an own implementation of the FDC parametrization and including the absorption by the extragalactic background light (Φ_{model}) with the 99% C.L. flux upper limits (Φ) derived in this work. For the objects 1ES 1959+650, H 1426+428 and 1ES 2344+514 fluxes are given. Objects printed in boldface show upper limits below the predicted values. In case of 1ES 0647+250 a redshift of 0.200 was assumed in order to be able to calculate the EBL absorption.

object	z	$\Phi_{\text{model}}/10^{-12}$		$\Phi/10^{-12}$		
		$\gamma \text{ cm}^{-2} \text{ s}^{-1}$		spectral index α		
		FDC	FDC+EBL	2.0	2.5	3.0
H 1722+119	0.018	36.98	20.53	<3.84	<3.62	<3.41
1ES 2344+514	0.044	18.58	4.72	= 0.58	= 0.57	= 0.56
Mkn 180	0.046	19.00	4.56	<1.64	<2.00	<2.45
1ES 1959+650	0.047	18.01	4.20	= (1.0 – 51.9)		
3C 371	0.050	12.41	2.80	<2.51	<3.09	<3.81
I Zw 187	0.055	12.40	2.25	<1.56	<1.51	<1.47
1ES 2321+419	0.059	4.85	0.75	<0.60	<0.56	<0.53
BL-Lacertae	0.069	1.66	0.22	<4.51	<4.73	<4.96
1ES 1741+196	0.083	7.10	0.55	<1.33	<1.29	<1.25
PKS 2155-304	0.116	2.40	0.07	<1.60	<3.83	<9.16
1ES 1118+424	0.124	2.36	0.05	<4.18	<4.12	<4.06
1ES 0145+13.8	0.125	1.16	0.02	<1.19	<1.11	<1.04
1H 0658+595	0.125	2.49	0.05	<0.98	<1.02	<1.06
H 1426+428	0.129	2.32	0.04	= 0.69		
1ES 1212+078	0.130	2.74	0.05	<2.98	<2.86	<2.74
1ES 0806+524	0.138	1.85	0.03	<4.63	<4.84	<5.05
1ES 0229+200	0.139	2.25	0.03	<2.99	<2.87	<2.75
RBS 0958	0.139	2.42	0.03	<5.30	<4.88	<4.50
1ES 1255+244	0.140	1.12	0.01	<2.03	<1.97	<1.91
1ES 0323+022	0.147	1.97	0.02	<0.71	<0.71	<0.71
OQ 530	0.152	0.23	$3 \cdot 10^{-3}$	<1.58	<1.67	<1.77
1ES 1440+122	0.162	1.69	0.01	<1.37	<1.31	<1.26
PKS 0829+046	0.180	0.03	$2 \cdot 10^{-4}$	<0.96	<0.96	<0.96
PG 1218+304	0.182	1.24	$5 \cdot 10^{-3}$	<2.24	<2.06	<1.88
1ES 0347-121	0.185	0.83	$3 \cdot 10^{-3}$	<7.50	<9.07	<10.96
1ES 0927+500	0.186	1.06	$3 \cdot 10^{-3}$	<1.02	<0.98	<0.95
PKS 2254+074	0.190	0.06	$2 \cdot 10^{-4}$	<0.89	<0.85	<0.80
MS 0317+1834	0.190	1.00	$3 \cdot 10^{-3}$	<2.37	<2.12	<1.89
1ES 0647+250	0.200	0.83	$2 \cdot 10^{-3}$	<2.61	<2.31	<2.04
1ES 1011+496	0.200	0.29	$7 \cdot 10^{-4}$	<1.84	<1.85	<1.87
1ES 0120+340	0.272	0.37	$8 \cdot 10^{-5}$	<0.72	<0.66	<0.60
2E 0414+0057	0.287	0.22	$3 \cdot 10^{-5}$	<2.18	<2.19	<2.20
S5 0716+714	0.300	0.21	$2 \cdot 10^{-5}$	<4.95	<6.22	<7.81
3C 66A	0.444	0.11	$1 \cdot 10^{-7}$	<3.29	<3.03	<2.80
PKS 0219-164	0.698	0.04	$5 \cdot 10^{-12}$	<3.29	<4.39	<5.86

below the value predicted by the FDC parametrization alone. But including the absorption by the EBL the predicted value is much lower than the observed flux (FDC+EBL). The observed flux level from 1ES 2344+514 is lower than the predicted value by a factor of 30 (only FDC) resp. 8 (FDC+EBL). However, this object has shown flux levels in the earlier Whipple data which exceeded the flux observed by HEGRA by a factor of 20, which shows that during HEGRA observations 1ES 2344+514 was indeed not in a flaring state. The SSC model of Costamante & Ghisellini (2002) predicts flux values

well below the observed upper limits. Most of these predicted values would only be detectable with much longer exposure times or with the next generation of Cherenkov telescopes.

7. Summary

A data set of 54 Active Galactic Nuclei observed with the HEGRA IACT system between 1996 and 2002 has been analysed. The two objects 1ES 1959+650 and H 1426+428 are meanwhile well established sources of TeV γ -radiation. The evidence for TeV γ -rays from 1ES 2344+514 is a confirmation of the detection of this object by the Whipple collaboration. The detection of TeV γ -rays from M87 would be, if confirmed, the first detection of photons in the TeV energy regime from an AGN of an object not commonly classified as a BL Lac object. Upper limits have been derived for all other 50 objects. Table 6 summarizes the results for the most significant excesses seen in this data set. Comparisons with different model predictions indicate that a higher sensitivity is needed to be able to constrain the models.

A further step towards understanding the involved acceleration mechanisms and of the AGN class as a whole as well as of the absorption by the extragalactic background radiation field is expected from further observations of AGN over a wide range of redshifts and especially BL Lac type objects with the next generation of Cherenkov telescopes (partly already in operation) and with future instruments. With the reduction of the energy threshold towards 100 GeV the effect of the absorption by the extragalactic background light will become less important for objects located at low redshift. Thus, the uncertainties in the interpretation of observations induced by this effect will be less important.

Acknowledgements. The support of the German Federal Ministry for Research and Technology BMBF and of the Spanish Research Council CICYT is gratefully acknowledged. GR acknowledges receipt of a von Humboldt fellowship. We thank the Instituto de Astrofísica de Canarias (IAC) for the use of the HEGRA site at the Observatorio del Roque de los Muchachos (ORM) and for supplying excellent working conditions on La Palma. This research has made use of the SIMBAD database, operated at CDS, Strasbourg, France and of the NASA/IPAC Extragalactic Database (NED) which is operated by the Jet Propulsion Laboratory, California Institute of Technology, under contract with the National Aeronautics and Space Administration.

References

- Aharonian, F., Daum, A., Hermann, G. et al., 1997, A&A, 327, L5
 Aharonian, F., Akhperjanian, A.G., Barrio, J.A., et al., 1999a, A&A 349, 11-28
 Aharonian, F., Akhperjanian, A.G., Barrio, J.A., et al., 1999b, A&A 349, 29-44
 Aharonian, F., Akhperjanian, A.G., Andronache, M., et al., 1999c, A&A 350, 757
 Aharonian, F. A. 2000, New Astronomy, 5, 377
 Aharonian, F., Akhperjanian, A.G., Barrio J.A., et al., 2001a, A&A 366, 62
 Aharonian, F., Akhperjanian, A.G., Barrio J.A., et al., 2001b, A&A 366, 746
 Aharonian, F., 2001, Proc. of the 27th ICRC, Hamburg, Highlight Papers, 250, astro-ph/0112314
 Aharonian, F. A., 2002, MNRAS, 332, 1, 215
 Aharonian, F., Akhperjanian, A.G., Beilicke, M., et al., 2002a, A&A, 393, 89
 Aharonian, F., Akhperjanian, A., Barrio, J., et al., 2002b, A&A, 384, L23
 Aharonian, F., Akhperjanian, A. G., Beilicke, M., et al., 2003a, A&A, 403, 523
 Aharonian, F., Akhperjanian, A. G., Beilicke, M., et al., 2003b, A&A, 403, L1
 Aharonian, F., Akhperjanian, A. G., Beilicke, M., et al., 2003c, A&A, 406, L9
 Bai, J.M. & Lee, M. G., 2002, ApJ, 549, L173
 Baltz, E. A., Briot, C., Salati, P., et al., Phys.Rev. D61 023514, 2000.
 Bicknell, G. V. & Begelman, M. C., 1996, ApJ, 467, 597
 Biermann, P.L., Ahn, E., Medina-Tanco, G., Stanev, T., astro-ph/9911123, astro-ph/0008063 and Nucl.Phys. B Proc.Suppl. 87 (2000) 417-419
 Bradbury, S. M., Deckers, T., Petry, D., et al., 1997, A&A 320, L5
 Catanese, M., Akerlof, C. M., Badran, H. M., et al., 1998, ApJ, 501, 616
 Chadwick, P. M., Lyons, K., McComb, T.J.L., et al., 1999, ApJ, 513, 161
 Costamante, L., Ghisellini, G., Giommi, P., et al., 2001, A&A, 371, 512
 Costamante, L., & Ghisellini, G., 2002, A&A, 384, 56
 Daum, A., Hermann, G., Hess, M., et al., 1997, Astroparticle Physics, 8, 1
 de la Calle Perez, I., Bond, I.H., Boyle, P.J., et al., 2003, Proc. of the 28th ICRC, Tsukuba, Vol. 5, 2571
 Djannati-Ataï, A., Piron, F., Barrau, A., et al., 1999, A&A, 350, 17
 Djannati-Ataï, A., Khelifi, B., Vorobiov, S., et al., 2002, A&A, 391, L25
 Djannati-Ataï, A., 2003, Proc. of the 28th ICRC, Tsukuba, Vol. 5, 2575
 Donato, D., Ghisellini, G., Tagliaferri, G. & Fossati, G., 2001, A&A, 375, 739
 Elvis, M., Plummer, D., Schachter, J. et al., 1992, ApJS, Vol. 80, no. 1, 257, May issue
 Fossati, G., Marashi, L., Celotti A., Comastri, A., Ghisellini, G., 1998, MNRAS, 299, 433
 Ginzburg, V. L. & Syrovatskii, S. I., 1965, ARA&A, 3, 297
 Giommi, P., Padovani, P., Perlman, E., et al., 2000, MNRAS, 317, 743G
 Götting, N. & the HEGRA collaboration, 2003, to appear in the Proc. of the EPS 2003 conf., Aachen, also astro-ph/0310308
 Helene, O., 1983, Nucl. Instr. Meth., 212, 319
 Hofmann, W., Jung, I., Konopelko, A., et al., 1999, Astroparticle Physics, 12, 135
 Horan, D., Badran, H. M., Bond, I. H., et al., 2002, ApJ, 571, 753
 Horan, D., Catanese, M.A., Bond, I.H. et al., 2003, Proc. of the 28th ICRC, Tsukuba, Vol. 5, 2567
 Jones, T.W., O'Dell, S.L. & Stein, W.A., 1974, ApJ, 188, 353
 Kolmogorov, A.N., 1933, Giornale Istituto Italiano Attuari 4, 83
 Konopelko, A., Hemberger, M., Aharonian, F., et al., 1999a, Astroparticle Physics, 10, 275
 Konopelko, A., Kettler, J., and the HEGRA Collaboration, 1999b, Proc. of the 26th ICRC, Salt Lake City, Vol. 3, 426
 Krawczynski, H., Sambruna, R., Kohnle, A., et al. 2001, ApJ, 559, 187
 Li, T. & Ma, Y., 1983, ApJ, 272, 317
 Mannheim, K. 1993, A&A, 269, 67

Table 6. This Table summarizes the results of the present analysis for the most significant objects from the sample of 54 AGN observed with the system of stereoscopic Cherenkov telescopes. The number of on- and off-events as well as significance S , fluxes in units of the Crab Nebula flux (F) and in units of 10^{-12} photons $\text{cm}^{-2}\text{s}^{-1}$ (Φ) above the energy threshold E_{thr} of the observation are given.

object	N_{on} [#]	αN_{off} [#]	S [σ]	E_{thr} [TeV]	F [Crab]	Φ [10^{-12} photons $\text{cm}^{-2}\text{s}^{-1}$]
1ES 1959+650	1212	454	28.0	1.32	0.06 – 2.9	0.6 – 30.5
H 1426+428	836	654	6.6	0.91	0.03	0.8
1ES 2344+514	235	171	4.4	0.97	0.03	0.6
M 87	241	184	3.9	0.88	0.04	0.8

- Mirzoyan, R., Kankanian, R., Krennrich, F., et al., 1994, Nucl. Instr. Meth. A 351, 513
- Mücke, A. & Protheroe, R. J. 2001, Astroparticle Physics, 15, 121
- Neshpor, Y. I., Stepanyan, A.A., Kalekin, O.P., et al., 1998, Astr. Lett., 24, 134
- Neshpor, Y. I., Chalenko, N.N., Stepanian, A.A et al., 2001 Astr. Rep., 45, 249
- Nishiyama, T., Chamoto, N., Chikawa, M., et al., 1999, Proc. of the 26th ICRC, Salt Lake City, Vol. 3, 370
- Nikishov, A.I., 1962, Sov. Phys. JETP 14, 393
- Padovani, P. & Giommi, P., 1995, MNRAS, 277, 1477
- Petry, D., Bradbury, S. M., Konopelko, A., et al., 1996, A&A 311, L13
- Piron, F., Djannati-Ataï, A., Punch, M., et al., 2001, A&A, 358, 895-906
- Prahl, J., 1999, astro-ph/9909399
- Protheroe, R. J., Donea, A.-C., Reimer, A., 2003, Astroparticle Physics, Volume 19, 559
- Primack, J. R., Somerville, R. S., Bullock, J. S., & Devriendt, J. E. G. 2001, High Energy Gamma-Ray Astronomy, AIP Conf. Proc., 558, 463
- Pühlhofer, G., Bolz, O., Götting, N., et al. 2003, Astroparticle Physics 20, 267
- Punch M., Akerlof, C.W., Cawley, M.F., et al., 1992, Nature, 160, 477
- Quinn, J., Akerlof, C. W., Biller, S., et al., ApJ, 456, L83, 1996
- Rees, M.J., 1967, MNRAS, 135, 345
- Rees, M.J., 1984, ARA&A, 22, 471
- Reimer, A., Protheroe, R.J., & Donea, A.-C., 2003, Proc. of the 28th ICRC, Tsukuba, Vol. 5, 2631
- Sambruna, R., Aharonian, F.A., Krawczynski, H., et al., 2000, ApJ, 538, 127
- Schachter, J. F., Stocke, T. J., Perlman, E., et al., 1993, ApJ, 412, 541
- Pohl, M. & Schlickeiser, R. 2000, A&A, 354, 395
- Sikora, M., AIP Conf.Proc. 558 (2001) 275-288
- Stecker, F. W., de Jager, O. C., Salamon, M. H., 1996, ApJ, 473, L75
- Stickel, M., Meisenheimer, K. & Kuehr, H., 1994, A&AS, 105, 211
- Tinyakov, P. G. & Tkachev, I. I., 2001, JETP Letters, 74, 445
- Ue-Li Pen, 1996, A&A Suppl. Ser., 120, 49
- Urry, C. M., Padovani, P., 1995, PASP, 107, 803
- Véron-Cetty & Véron, 2001, A&A, 374, 92

Table 7. List of all objects of the HEGRA AGN data sample. The J2000 coordinates are given as well as redshift and object type (following Stickel et al. (1994); Padovani & Giommi (1995); Véron-Cetty & Véron (2001)). The results of the analysis presented here are summarized. In case of the objects deviating significantly from the background expectation the flux is given in units of the Crab Nebula flux. For all other objects upper limits on the integral flux in units of the Crab Nebula flux ($F_{UL}^{99\%}$) and in units of 10^{-12} photons $\text{cm}^{-2}\text{s}^{-1}$ ($\Phi_{UL}^{99\%}$) are given.

object	α_r	δ	z	type	T	E_{thr}	S	$F_{UL}^{99\%}$	$\Phi_{UL}^{99\%}/10^{-12}$	F
	(hh mm ss)	(dd mm ss)								
1ES 0647+250	06 50 46.6	+25 03 00	—	BL	4.1	0.78	0.5	0.13	3.35	
MG 0509+0541	05 09 26.0	+05 41 35	—	BL	15.8	0.96	1.3	0.11	1.92	
M 87	12 30 49.4	+12 23 28	0.004	F1	70.0	0.88	3.9			0.04
NGC 315	00 57 48.9	+30 21 08	0.016	F1/2	14.6	0.86	-0.3	0.05	1.03	
NGC 1275	03 19 48.2	+41 30 42	0.018	F1	87.6	0.85	-0.3	0.03	0.68	
H 1722+119	17 25 04.5	+11 52 15	0.018	BL	5.1	0.89	1.7	0.21	4.31	
PKS 2201+04	22 04 17.7	+04 40 03	0.028	S1	17.8	0.95	1.7	0.08	1.40	
V Zw 331	03 13 57.0	+41 15 37	0.029	BL	4.1	0.87	-0.2	0.09	1.93	
NGC1054	02 42 15.0	+18 13 00	0.032	G	57.9	0.86	-1.7	0.02	0.37	
3C 120	04 33 12.0	+05 21 15	0.033	F1	25.4	0.93	-0.7	0.05	0.86	
NGC 4151	12 10 32.7	+39 24 19	0.033	S1.5	7.0	0.79	-0.4	0.07	1.79	
UGC01651	02 09 38.5	+35 47 51	0.037	G	14.3	0.79	1.3	0.07	1.62	
UGC03927	07 37 30.0	+59 41 03	0.041	F2	6.3	1.09	-2.4	0.09	1.32	
1ES 2344+514	23 47 04.9	+51 42 17	0.044	BL	72.5	0.97	4.4			0.03
Mkn0180	11 36 26.4	+70 09 27	0.046	BL	9.8	1.50	-0.6	0.12	1.09	
1ES 1959+650	19 59 59.9	+65 08 54	0.047	BL	163.7	1.32	28.0			0.06 – 2.9
3C 371.0	18 06 50.7	+69 49 28	0.050	BL	5.4	1.52	-0.4	0.19	1.65	
4C +37.11	04 05 49.3	+38 03 32	0.054	S	6.7	0.80	-2.0	0.05	1.17	
I Zw 187	17 28 18.6	+50 13 10	0.055	BL	16.0	0.94	1.9	0.09	1.66	
Cyg-A (3C 405.0)	19 59 28.5	+40 44 02	0.057	F2	59.0	0.91	-0.2	0.03	0.64	
1ES 2321+419	23 23 52.5	+42 10 55	0.059	BL	22.3	0.89	-1.6	0.03	0.67	
3C 192.0	08 05 35.0	+24 09 50	0.060	F2	2.9	0.93	0.3	0.20	3.78	
4C+31.04	01 19 35.0	+32 10 50	0.060	FR	3.0	0.76	-0.3	0.14	3.83	
BL-Lacertae	22 02 43.3	+42 16 40	0.069	BL	26.7	1.10	3.0	0.28	4.10	
1ES 1741+196	17 43 57.8	+19 35 09	0.083	BL	10.2	0.94	0.3	0.07	1.41	
4C+01.13	05 13 52.5	+01 57 10	0.084	F2	7.7	1.01	-0.2	0.10	1.73	
PKS 2155-304	21 58 52.0	-30 13 32	0.116	BL	1.8	5.72	0.0	0.27	0.28	
1ES 1118+424	11 20 48.1	+42 12 12	0.124	BL	2.0	0.97	0.3	0.24	4.31	
1ES 0145+13.8	01 48 29.8	+14 02 19	0.125	BL	3.2	0.87	1.1	0.06	1.37	
1H 0658+595	07 10 30.1	+59 08 20	0.125	BL	33.7	1.08	-0.4	0.06	0.91	
H 1426+428	14 28 32.5	+42 40 25	0.129	BL	258.5	0.91	6.6			0.03
3C197.1	08 21 32.6	+47 02 46	0.130	QSO	15.0	0.96	-0.4	0.05	0.86	
1ES 1212+078	12 15 11.2	+07 32 02	0.130	BL	2.4	0.92	-0.6	0.17	3.24	
1ES 0806+524	08 09 49.2	+52 18 58	0.138	BL	1.0	1.09	-0.1	0.29	4.25	
1ES 0229+200	02 32 48.7	+20 17 17	0.139	BL	3.0	0.92	1.0	0.17	3.25	
RBS 0958	11 17 06.3	+20 14 06	0.139	BL	3.8	0.85	2.7	0.28	6.23	
1ES 1255+244	12 57 32.0	+24 12 39	0.140	BL	5.9	0.94	0.1	0.12	2.16	
MS1019.0+5139	10 22 11.0	+51 24 00	0.141	S	17.5	0.92	0.1	0.07	1.35	
1ES 0323+022	03 26 13.9	+02 25 14	0.147	BL	14.3	1.00	-1.5	0.04	0.71	
OQ 530	14 19 46.6	+54 23 14	0.152	BL	9.4	1.12	0.4	0.10	1.41	
3C 273.0	12 29 06.7	+02 03 08	0.158	FR	12.2	1.15	-0.3	0.09	1.25	
1ES 1440+122	14 42 48.4	+12 00 39	0.162	BL	13.1	0.92	-0.9	0.08	1.49	
PKS 0829+046	08 31 48.9	+04 29 39	0.180	BL	18.0	1.00	0.5	0.06	0.96	
PG 1218+304	12 21 22.0	+30 10 37	0.182	BL	3.9	0.84	-0.3	0.12	2.67	
1ES 0347-121	03 49 23.0	-11 59 26	0.185	BL	1.9	1.46	1.8	0.56	5.14	
1ES 0927+500	09 30 37.6	+49 50 24	0.186	BL	13.3	0.94	0.2	0.06	1.08	
PKS 2254+074	22 57 17.3	+07 43 12	0.190	BL	16.3	0.90	-0.5	0.05	0.99	
MS0317.0+1834	03 19 51.9	+18 45 35	0.190	BL	2.7	0.80	-0.5	0.12	2.96	
1ES 1011+496	10 15 04.2	+49 26 00	0.200	BL	2.0	1.02	-1.3	0.11	1.80	
1ES 0120+340	01 23 08.9	+34 20 50	0.272	BL	18.9	0.83	-1.2	0.04	0.87	
2E 0414+0057	04 16 52.5	+01 05 23	0.287	BL	4.5	1.01	0.6	0.13	2.16	
S5 0716+714	07 21 53.4	+71 20 36	0.300	BL	1.7	1.58	0.7	0.38	3.13	
3C 066A	02 22 39.6	+43 02 07	0.444	BL	1.3	0.85	-0.2	0.17	3.87	
PKS 0219-164	02 22 01.0	-16 15 16	0.698	BL	1.7	1.78	-1.7	0.27	1.85	